Transient Electrical Behaviour of the TF Superconducting Coils of Divertor Tokamak Test Facility During a Fast Discharge

G. Messina, C. R. Lopes, P. Zito, A. Di Zenobio, C. Fiamozzi Zignani, A. Lampasi, L. Morici, G. Ramogida, G. Tomassetti, G. Ala, G. Zizzo

***Abstract*— The paper is focused on the electromagnetic analysis of the Toroidal Field superconducting coils (TFCs) of the Divertor Tokamak Test facility (DTT) when electrical transients occur in the TFCs system: for example, during the operations of the Fast Discharge Units (FDUs) and considering also, the simultaneous occurrence of a fault condition. During the FDU intervention, a transient voltage excitation lasting few milliseconds occurs at the TFC terminals and it electrically stresses the insulations of TFCs itself. To investigate the voltage distribution across, inside and between different Double Pancakes (DPs) of each TFC, a lumped parameters circuital model has been developed and implemented in *Ansys Simplorer* simulation environment. This model includes both the detailed sub-model of each TFC and FDU. The transient analyses have been carried out for two different scenarios: a reference one and a failure scenario, considering three different fault resistance values and also two different values of the resistance connecting the TF case to ground. In order to verify the correct sizing of the coil insulation and the TF case-to-ground resistance value inserted in the circuit of each TFC, the voltages of each TFC (terminal-to-terminal, terminal-to-ground, across of adjacent DPs and between other circuit points) were computed in the time domain (in the range of milliseconds) for both scenarios. An overview of calculations and simulation results is presented and discussed, pointing out a high sensitivity of fault conditions and of overvoltage values and addressing mitigation strategies.**

***Index Terms*— DTT, FDU, Toroidal Field Model Coil (TFMC), Central Solenoid Model Coil (CSMC), Electromagnetic modelling, Fast Discharge, Voltage distribution, Ground fault conditions**

I. Introduction

The DTT is a facility under construction in the Frascati ENEA research centre (Rome). The DTT magnetic system consists of: 18 TFCs; 1 Central Solenoid (CS) divided into 6 independent modules, aimed also at plasma shaping; 6 Poloidal Field (PF) coils; structural and common components; 8 In-Vessel copper Coils (IVCs) [1-2]. The 18 TFCs are connected in series and three Fast Discharge Units (FDUs) are inserted in this power circuit, each of which drives a group of 6 TFCs. The FDU is a key component for the protection of the magnets as it allows the rapid discharge of the magnets in case of a quench, of a fault or when a failure of the Toroidal Field Power Supply (TFPS) occurs; therefore, the reliability of the FDU is of primary importance as the safety of the superconducting magnets depends on it. In previous works [3] it has been demonstrated how the discharge of the FDU can take place with passive elements (fixed resistors) or with active elements (IGCTs progressively disconnected through the discharge time) allowing a reduction of the maximum voltage of 20%, the reduction of discharge time of TFCs of 72% and the possibility of installing only three FDUs instead of six with considerable advantages from the point of view of thermal and electrical parameters. The model, the mathematical approach and the control system have been simulated with Matlab and extensively described in [3]. The voltage across each TFC is negligible during the normal operation, but in case of quench it increases very fast and the TFCs must be discharged to avoid their damage. The opening signal is sent to the FDU when a quench is detected; this phenomenon occurs when a superconductor passes from the superconducting phase to normal conduction, for example, due to external perturbations over the conductors: it involves the power losses and consequent risk of serious damage of the superconducting material. For this reason, the operation of the FDU must be as quick as possible once the fault or the quench is identified and the discharge of the magnets must take place in total safety and with maximum efficiency. As it was extensively described in [3], every time that the crowbar (an electrical breaker) is activated to bypass the TFPS, a trigger signal will be send to each FDU. The hybrid Circuit Breaker (CB) of each FDU, composed by a mechanical By-Pass Switch (BPS) and a Static Circuit Breaker (SCB), will connect in series the TFC to the dump resistors (DRs) in order to dissipate the energy associated to the coils magnetic field (Fig.1). The discharge of the TFC current on the dump resistor causes transient voltage excitation in the range of milliseconds across the coil itself: the voltage waveform may lead to internal oscillations and overvoltage within the coil [4-6]. This waveform voltage is characterized by a peak value that occurs during the first instants of the discharge and by a series of damped oscillations before decreasing to zero with an exponential (*passive* discharge) or linear (*active* discharge) trend, dependent on the time constant and thus on

G. Messina, P. Zito, A. Di Zenobio, C. Fiamozzi Zignani, A. Lampasi, L. Morici, G. Ramogida and G. Tomassetti are with ENEA for EUROfusion, 00044 Frascati, Roma, Italy. Corresponding author: G. Messina (e-mail: giuseppe.messina.fra@enea.it, phone: +39 0694005674, fax: +39 694006119).

C. R. Lopes, G. Ala and G. Zizzo are with Department of Engineering, University of Palermo, Palermo, Italy (e-mail: carmeloriccardo.lopes@unipa.it).

P. Zito, A. Lampasi, G. Ramogida and G. Messina are with ENEA, DTT S. c. a r. l., Frascati (Italy) (e-mail: pietro.zito@enea.it).

the dump circuit parameters. The peak value of the voltage at the coil terminals depends on the switch technology of each FDU and on the stray impedances of the connections between the aforementioned switch and the dump resistor bank: its approximate value can be estimated from the energy stored in its magnetic field, from the operating current and from the discharge time constant, τ. In addition, fault cases may increase the voltage above the values of a normal sequence of a fast discharge. Therefore, detailed calculations are necessary to predict the transient electrical behaviour of the coils in terms of electrical stress at three insulation levels: the insulation between adjacent turns belonging to the same pancake; the insulation between adjacent DPs; the ground insulation between the whole Winding Pack (WP) and the grounded coil case. The simulation studies presented in this paper are based on several measurements and works realized in the recent past [4], [5], [6] and [7]. In these works, the authors refer to several experimental measurements carried out on ITER TFMC and on CSMC to study and validate models of the electrical behaviour of superconducting large fusion coils and their transient overvoltage. Thus, the simulation strategies implemented here are based on the referred verified assumption, and the described model has been developed and suited for the DTT TFCs design characteristics. The analysis strategy and results are described in the following Sections.

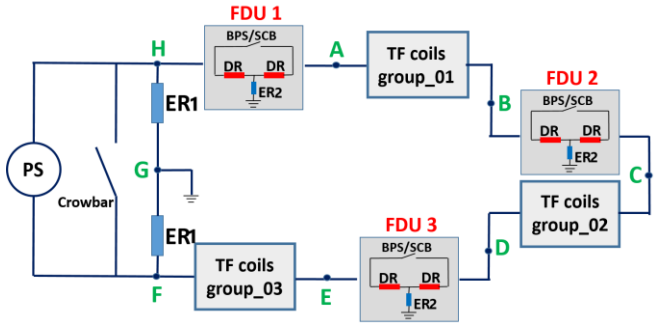

Fig.1. Electrical circuit of TFCs system (qualitative description).

II. Analysis Objective and Strategy

The object of our investigation is the simulation of the electromagnetic behaviour during the transients that occur in the TFCs system in concurrence with the Fast Discharge and with the simultaneous occurrence of a fault condition. Predicting the TFC behaviour in these operating conditions means estimating the propagation of the voltage waveform, across and among adjacent DPs of each TFC, which is useful to achieve the goal of this analysis: to verify the correct sizing of the coil insulation and of the TF case-to-ground resistance ($R_{case\text{-}to\text{-}gnd}$) value inserted in the circuit of each TFC.

The analysis strategy consists of three main parts: the Finite Element Methods (FEM) calculations; the circuital model assembly and implementation; the circuital analysis in time domain. The basis for the modelling are the TFC geometry, TFC materials and the design of its electrical circuit. The WP FEM model of a TFC has been used to calculate the self and mutual inductance coefficients at DC (see following paragraph). In order to assemble the TFC circuital model, the inductances matrix has been implemented as a coupling matrix together with the capacitances and the resistances, analytically estimated. Each single TFC circuit has been then modelled as a sub-circuit as well as each FDU: the latter includes the electrical parameters to simulate the operations of its hybrid CBs (mechanical and static switch) and an *active* discharge by DRs [3]. All sub-circuit just described have been connected in series to each other and to the TFPS. By varying the $R_{case\text{-}to\text{-}gnd}$, the voltage waveforms distribution were investigated for two different scenarios:

- reference scenario: the synchronous switching of the FDUs;
- failure scenario: a delayed intervention of a FDU and an additional ground fault.

The terminal-to-terminal voltage, the terminal-to-ground voltage, the voltage across adjacent DPs and any overvoltage that may occur between other circuit points of each TFC were computed in time domain (in the range of milliseconds) for both scenarios.

III. FEM Models Descriptions

In order to estimate the TFC inductance value, a FEM model consisting of 18 TFCs system has been implemented in *Ansys Maxwell* 3D. As the coil cross section of each TF has been defined to be a solid conductor, the result of the magneto-static analysis was the 18x18 matrix of self (L_{TF} = 45.71 mH) and mutual inductance coefficients. This result has been used to switch from a 3D analysis to a 2D axisymmetric one.

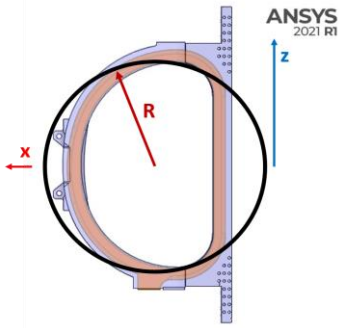

Fig.2 Schematic view of a D- and Circular shaped TFC.

A. From D-shaped to Circular-shaped geometry

The WP of each D-shaped TFC consists of 84 turns grouped into 5 DPs: the three central double pancakes have 18 turns each while the two outer DPs have 15 turns each. The superconducting CICC (cable in conduit conductor), used to wind the TFC, is contained into a rectangular section steel jacket. A fiberglass tape is then wrapped around the jacket so as to create 2.0 mm of electrical insulation between adjacent conductors while a further 0.5 mm insulating tape is wrapped around each DP. An alternate fiberglass/polyamide layer is then wrapped over the entire WP section in order to create an electrical insulation layer (thickness of 2.0 mm) on which, subsequently, a layer of conductive paint is applied to have an equipotential surface for the electric field streamlines [8]. The WP is then inserted inside a stainless-steel case, connected to ground by a resistance ($R_{case\text{-}to\text{-}gnd}$), with a 4.0 mm clearance

which is filled by fiberglass. After all these operations, all the magnet is filled by epoxy resin by a Vacuum Pressure Impregnation process and then cured. Curing leads to polymerization and hardening: the whole process determines the electrical performance of the insulation. The $R_{case\text{-}to\text{-}gnd}$ parameter will be set in a range within 1 mΩ and 100 mΩ: the final value will be the result of the circuit analysis reported below. In order to study the effect of representing each turn with more than one electric element (R, L, C and so), a Circular-shaped TFC with an internal radius of R = 1.68 m has been considered to simplify the D-shaped TFCs modelling (Fig. 2). This coil, having the same case and WP cross-section of the D-shaped TFC, has been then implemented in *Ansys Maxwell* 3D and the magneto-static analysis returned a self-induction coefficient, (L_C = 46.6 mH), 2% different only from that of the D-shaped coil (L_D = 45.71 mH). Really, the magnetic field of a D-shaped TFC is slightly different from that of circular one (fig. 2) but, as obtained in terms of self-inductance parameters, this difference is acceptable since the aim of the simulation is the inductance coefficients matrix estimation.

TABLE I
ELECTRICAL CONDUCIBILITY @ CRYOGENIC TEMPERATURE.

Domain	Material	Value
case	Stainless- steel	$1.88 \cdot 10^6$ (S/m)
superconductor	LTS	$1 \cdot 10^{10}$ (S/m)
jacket	Stainless- steel	$1.88 \cdot 10^6$ (S/m)
vacuum	Air	0

B. An axisymmetric 2D model

Starting from the Circular-shaped coil and with reference to the geometric parameters of the superconducting cable used to wind the aforementioned coil, the axisymmetric 2D model of the WP + Case has been implemented in *Ansys Maxwell*. The shielding effect of the currents induced on the case is such that each TFC can be considered magnetically isolated. Therefore, as a first step, the passive structures (Vacuum Vessel and Stabilizing Plates) have been neglected and the computation time reduced. Considering that each turn is the whole of the superconductive (SC) strands and the jacket that surrounds them, the model has been divided into four domains: case, SC strands, jacket and vacuum (Fig. 3). Each of these domains is associated with a material appropriately chosen from those present in the *Ansys Maxwell* library, whose electrical conductivity values at cryogenic temperature have been reported in Table I. The result of the magnetostatic analysis was the 169x169 matrix (84 SC strands, 84 jacket, 1 case) of the self and mutual inductance coefficients of the WP whose range of values are indicated below:

- 11.1250 μH < L_{turn} < 12.6570 μH;
- 10.335 μH < L_{jacket} < 11.776 μH;
- L_{case} = 5.705 μH;
- 4.1043 μH < $M_{turn\text{-}to\text{-}turn}$ < 9.9293 μH;
- 4.1043 μH < $M_{turn\text{-}to\text{-}jacket}$ < 11.8710 μH;
- 4.7989 μH < $M_{turn\text{-}to\text{-}case}$ < 6.2316 μH;
- 4.7989 μH < $M_{jacket\text{-}to\text{-}case}$ < 6.2316 μH.

As well known, the values of inductance have strong frequency dependence caused by the induced currents in the stainless steel jacket surrounding the superconducting cable. The shielding effect on the magnetic field due to the induced currents on the jacket of the SC of each turn, has been highlighted in the transient analysis up to 50 Hz. This results in a reduction of the self and mutual inductance coefficients of the SC strands as the frequency increases.

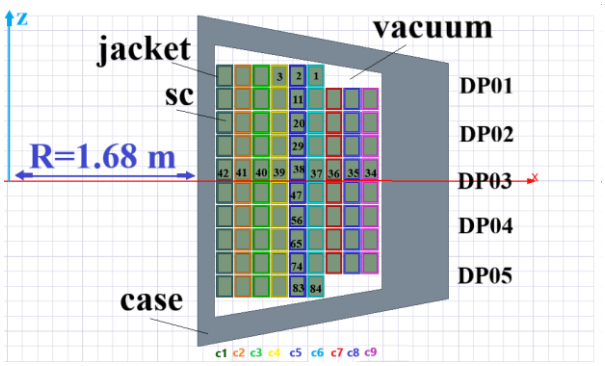

Fig.3. Axisymmetric 2D model of the WP in *Ansys Maxwell*.

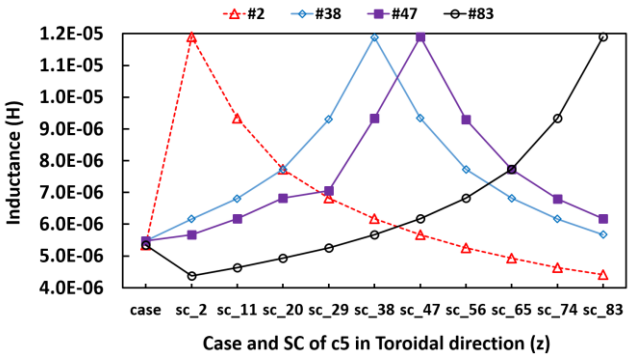

Fig.4. Comparison in DC of the mutual coupling coefficients regarding some turns (SC_2, SC_38, SC_47, SC_83) of column 5.

Comparison in DC of the mutual coupling coefficients regarding some turns (SC_2, SC_38, SC_47, SC_83) of the column 5 (c5, see Fig. 4) shows that the turns regarding SC_38 and SC_47 of the DP03, placed in the central region of the WP, have higher values (Fig. 4).

IV. CIRCUITAL MODELS

A. TFC

The self and mutual inductance coefficients matrix, obtained from the magneto-static analysis in *Ansys Maxwell* 2D, was imported as a coupling matrix in *Ansys Simplorer*. Hence, this choice of taking into account the DC values of the inductance matrix will produce an overestimation of the resulting peak voltage as, at the transient, the frequency dependent inductance values will certainly be lower. Concerning Fig. 3, since the jacket surrounding the SC strands for each turn has been included in the model, as well as the casing, SC strands and jacket correspond to a pair of inductances and therefore, to a pair of terminals (electrical ports) each. The resulting box associated to the inductances matrix has 169 input and 169

output ports connected according to WP configuration. Each of the 84 turns have been modelled with two ohmic-inductive branches (R-L) connected in parallel:

- *sc_branch*: concerning the 420 strands of the superconducting cable;
- *steel_branch:* concerning the jacket of the superconducting cable (the eddy currents on the copper matrix are neglected).

The electrical parameters L_{steel}, $M_{sc\text{-}steel}$ and L_{sc}, indicated in Fig. 5, are obtained from the magneto-static analysis while R_{steel} parameter has been estimated analytically.

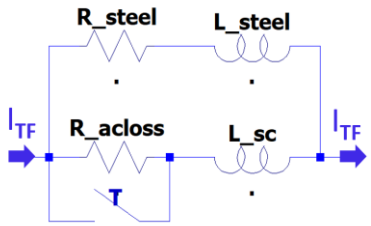

Fig.5. Electrical model associated to a single turn of the WP.

The $R_{\_acloss}$ parameter is the resistance whose power dissipated is associated to power losses in the superconducting material during the transient [9-10]. These losses take into account the superconducting material properties dependent to the magnetic field and can be considered as the sum of two contributions: the hysteresis losses, P_{hy}, and the coupling losses, P_{coupl}, expressed with the formulas (1) and (2) in W/m^3, respectively:

$$P_{hy} = \frac{2}{3\pi} d_{eff} \cdot A_{noCu} \int J_{noCu}(x,t) \cdot \dot{B}(x) dx = \alpha(I_{max}) \cdot \frac{dI}{dt} \quad (1)$$

$$P_{coupl} = \frac{1}{\mu_0} \cdot n\tau \cdot A_{noCu} \cdot B_i^2(t) = 9.15 \cdot 10^{-5} \cdot (\frac{dI}{dt})^2 \quad (2)$$

$$R_{\_acloss} = R_{hy} + R_{coupl} = \frac{Vol_{sc}}{\tau} \cdot [\frac{\alpha \cdot (I_{max})}{I_0} + \frac{9.15 \cdot 10^{-5}}{\tau}] \quad (3)$$

TABLE II
UNITS FOR CICC PROPERTIES

Symbol	Descriptions	Value
nτ	Cable time constant	250 ms
A_{noCu}	No-copper section in the conductor	133 mm^2
τ	Time constant	5 s
B_i	assumed here ~B_{ext}	
d_{eff}	Filament effective diameter	15 μm
I_0	TF coil current (maximum value)	42.5 kA
α(I_{max})	α(I_{max}) for I_0 = 42.5 kA	0.138

TABLE III
R_ACLOSS VALUES OF DIFFERENT TURNS

Turns #	Length [m]	Vol_{sc} [m^3]	R_{hy}^* [Ω]	R_{coupl} [Ω]	R_{acloss} [Ω]
c1	10.62	2.25e-04	1.460e-10	8.23e-10	9.687e-10
c2	10.77	2.28e-04	1.481e-10	8.34e-10	9.826e-10
c3	10.92	2.31e-04	1.502e-10	8.46e-10	9.964e-10
c4	11.07	2.34e-04	1.522e-10	8.58e-10	1.010e-09
c5	11.22	2.38e-04	1.543e-10	8.70e-10	1.024e-09
c6	11.38	2.41e-04	1.564e-10	8.82e-10	1.038e-09
c7	11.53	2.44e-04	1.585e-10	8.93e-10	1.052e-09
c8	11.68	2.47e-04	1.606e-10	9.05e-10	1.066e-09
c9	11.83	2.51e-04	1.627e-10	9.17e-10	1.08e-09

With reference to Fig. 3 and Table II, the R_{acloss} values for the turns of each column (c1, c2, ..., c9) of the WP have been calculated at the start of the discharge (t = 0) using formula (3) and reported in Table III. In this calculation, Vol_{sc} is the superconductor volume of each turn, while the TFC current, I_{TF}, has been supposed decreasing with a linear trend, $I_{TF} = I_0 \cdot [1-(t/\tau)]$ when the FDUs are triggered. The R_{acloss} obtained values were then inserted at the beginning of the discharge by means of the ideal switch, T (Fig. 5), and kept constant for the entire duration itself. The circuital model of a single TFC includes:

- the box of the inductances matrix;
- the resistances R_{acloss} and R_{steel} of each turn;
- the joint resistances (R_{joint} = *1 nΩ*) connecting adjacent DPs;
- the R_{paint} = *210 Ω* is 1/38th (each one of the 38 external turns in radial and toroidal direction) of the total value of 8 kΩ that has been assumed for the conductive paint applied onto the outer surface of the coil to homogenise the electrical field on it [11];
- the capacitances between turns and grounded parts;
- electrical parameters (R_{case}, L_{case}) of the case.

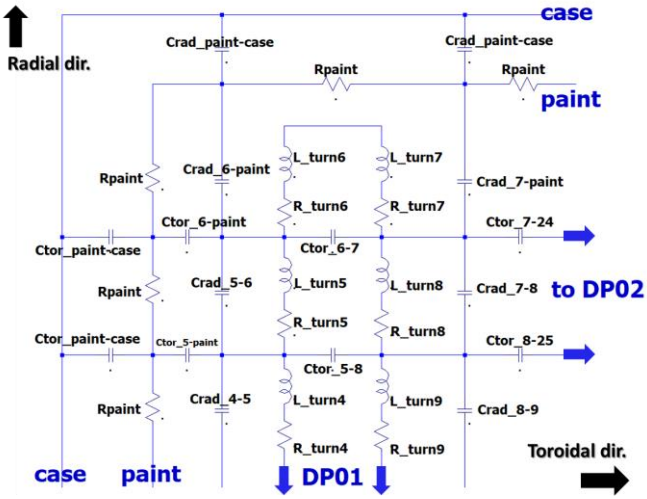

Fig.6 Simplified circuital configuration of a single TFC.

In Fig.6 a simplified circuital configuration of a single TFC is shown [12-18]. As the conductive paint layer and the case are electrically connected to each other and then to ground by means of a resistance, $R_{case\text{-}to\text{-}gnd}$, the paint-to-case capacitances have not been taken into account, while all other frequency independent capacitances are estimated analytically. All capacities in the toroidal direction (z-axis), C_{tor}, and in the radial direction (x-axis), C_{rad}, have been estimated by applying the formula of the flat capacitor and the cylindrical capacitor composed of two coaxial and concentric cylinders, respectively (see [3]). The range of the obtained results, in toroidal and radial direction, are reported below:

- 3 nF < $C_{turn\text{-}turn,tor}$ < 5 nF
- 0,3 nF < $C_{turn\text{-}paint,tor}$ < 3 nF
- 5 nF < $C_{turn\text{-}turn,rad}$< 6,5 nF
- 0,15 nF < $C_{turn\text{-}paint,rad}$< 5 nF

The broad ranges of the capacitance values come from different

position of the corresponding turns and of the outermost turns respect to the conductive paint layer, in both directions.

B. FDU

1) FDU's components and electric scheme

Regarding the electrical topology (Fig. 7), the FDU is composed by:

- Mechanical BPS: it conducts the current I_{TF} during normal operating conditions; therefore, it is always closed in the absence of faults.
- SCB: it conducts the current only during the opening process of the FDU as explained in detail later.
- DR: these are two fixed resistors in series connected and their middle point is ground connected by means an earthing resistance (ER2) of 160 Ω. Its role is to fix the middle point potential in order to divide the voltage to ground, and to limit the ground fault current when one FDU terminal is grounded. However, the temperature dependence of all resistances (DR and ER) is not considered. DRs are used to discharge the TFCs; in particular, the discharge can be *passive* when there is no variation of the equivalent resistance seen at the ends of the FDU (less efficient and slower process) or *active* if each DR is made up of 15 parallel branches of resistors in series to IGCT (Integrated Gate-Commutated Thyristor). The latter components, progressively disconnecting the branches according to the current thresholds, allow to have a variable resistance at the ends of the FDU in such a way to optimize the discharge process and decrease the total discharge time of the magnet to about 7 s (instead of 20 - 25 s for exponential discharge). Both types of discharges can be implemented within the model: a fast linear discharge in case of a quench of TFCs and a slow exponential discharge (classic R-L circuital behavior) in case of a quench of superconducting feeders. The reason for this choice is due to the attempt made not to excessively stress the superconducting magnets, both thermally and mechanically.
- Backup Pyrobreaker: it is a backup component that intervenes in extreme cases when there is a failure that does not allow the FDU to discharge the energy of the magnet and intervenes by opening the circuit with explosives.

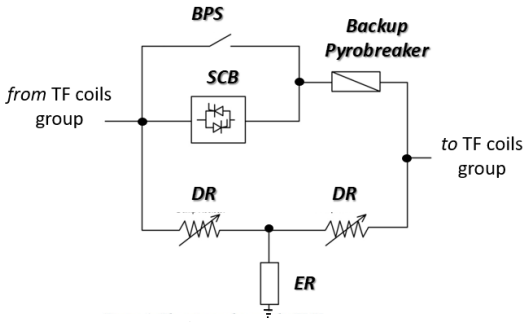

Fig.7. Electrical topology of FDU.

2) FDU discharge

When a quench occurs and it is recognized by the control data acquisition system (CODAS), the opening signal is commanded to the FDUs and the opening sequence is described as follows:

- During the normal conditions, the BPS is closed and conducts the rated current of 42.5 kA for the TFCs; the opening signal is sent to the BPS, which, being a mechanical switch, introduces its own delay before the opening sequence actually begins due to mechanical inertia. Once the switch begins to open, an arc current is established which is extinguished within Δt = *25-30 ms* (simulated according to the Mayr-Cassie model with some modifications described later).
- While the current decreases on the BPS, there is a progressive increase of the current on the SCB to which the conduction command has been given.
- When the current on the BPS reaches the zero value, the current flows progressively from the SCB to the DR and this discharge occurs by means of IGCTs (see next point).
- On the DR there are 15 branches in parallel consisting of fixed resistors and IGCTs as shown in Fig. 8. The IGCTs are controlled in current and at the start of the discharge on the DR they are all conducting, so the equivalent resistance is R_{DR} = *122 mΩ* (parallel of the 15 branch resistances): this is the minimum resistance value of the DR seen at the FDU terminals, since, during the discharge progress, single branches are disconnected by the IGCTs depending on the current circulating on the FDU.

In order to operate a linear discharge, in fact, the command to open an IGCT branch are given increasing the equivalent resistance R_{DR} at the ends of the FDU itself (for further details on the fault analysis and on the operating principle of the linear discharge, see [19]).

3) BPS Arc-modelling

This section is dedicated to the modelling and the simulation of the arc current on the BPS. As mentioned above, the BPS is a mechanical switch and therefore, when it is commanded to open, there is the formation of the arc current that flows between the poles of the switch itself. This current was modeled using Matlab-Simulink referring to the Mayr-Cassie model [20] with the parameters readjusted according to the technical requirements of the FDU; then, the arc resistances were implemented in the individual FDUs model in *Ansys Simplorer*. The Mayr-Cassie model is based on the following equations:

Mayr equation:

$$\frac{dg_m(t)}{dt} = \frac{1}{\tau_m}\left(\frac{i^2(t)}{P_0} - g_m(t)\right) \quad (5)$$

Cassie equation:

$$\frac{dg_c(t)}{dt} = \frac{1}{\tau_c}\left(\frac{i^2(t)}{u_c g_c} - g_c(t)\right) \quad (6)$$

The total arc resistance is:

$$R_{arc} = \frac{1}{g} = \frac{1}{g_m} + \frac{1}{g_c} \quad (7)$$

where g_m is the Mayr conductance, g_c is the Cassie conductance, τ_m is the Mayr time constant, τ_c is the Cassie time constant, $i(t)$ is the arc current, P_0 is the steady state power loss for

convection and radiation, u_c is the steady state arc voltage. Steady state arc voltage and steady state power loss were calculated from Paukert's parameters and studies [21]. This model, initially studied and validated on *Matlab-Simulink*, has been afterwards implemented in the *Ansys Simplorer* model to simulate the arc current on the mechanical BPS.

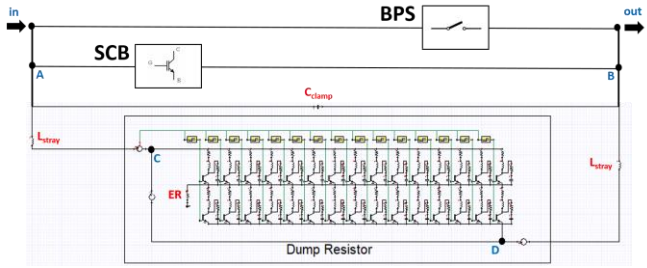

Fig.8. Circuital model of a FDU.

TABLE IV
MAYR-CASSIE SIMULATION PARAMETERS

Symbol	Explanations	Value
u_c	Steady state arc voltage	37.05 V
P_0	Steady state power loss	1.575 MW
τ_m	Mayr time constant	7 ms
τ_c	Cassie time constant	1.5 ms

The values of the arc parameters for the Mayr-Cassie simulation are shown in Table IV. The phenomenon described above is characterized by a considerable uncertainty, so the experimental value could be different from the simulated value up to 20-30%. Fig. 8 shows the FDU circuit model implemented in *Ansys Simplorer* in which the stray inductances of the DRs and of its connections to the SCB (L_{stray}) have been inserted: these components, which play an important role on voltage waveforms, have been set equal to 10 μH [22, 23]. Furthermore, to limit the peaks of transient voltages associated to the high TF current, a clamp capacitor of 3 mF has been connected in parallel to the SCB, while suitable snubber circuits have been positioned in each branch of the SCB and DR. The stray inductances and the clamp capacitors values, used for the simulation studies, are given by the DTT Power Supply team design.

C. TFCs system

The combination of circuital models of TFCs and FDUs have been used to implement the circuit model associated to the TFCs system. For $f = 1\ kHz$ the skin depth of the TFC case is about 1 cm, and, since the case is thicker than 1 cm, the effects of the induced magnetic field can be neglected at frequencies higher than 1 kHz. Because of this, each TFC could be modelled as a sub-circuit electrically connected but magnetically decoupled of each other in the range of frequencies 1 kHz ÷100 kHz. Each sub-circuit includes input and output ports for each DP and a case port to connect the TFC to ground by means a resistance, $R_{case\text{-}to\text{-}ground}$. To investigate the influence of this last parameter on the voltages waveform, the transient analyses were carried out with $R_{case\text{-}to\text{-}gnd} = 1\ m\Omega$ and with $R_{case\text{-}to\text{-}gnd} = 100\ m\Omega$.

The 18 sub-circuits are divided into three groups of six sub-circuits: all groups, their corresponding pairs of bus-bars and three FDU circuit are in series connected to a branch composed of the TFPS with the crowbar in parallel connected. The busbars have been modelled as a resistance ($R_{busbar} = 116\ \mu\Omega$) and an inductance ($L_{busbar} = 460\ \mu H$) in series connected both for inlet and outlet conductors (100 m length): the stray capacitances of the bus-bar and the electrical parameters of the superconducting feeders have not been taken into account. The TFPS has been modelled as a DC current source while the crowbar has been modelled as an ideal switch in parallel connected to two earthing resistances, $ER1 = 1\ k\Omega$ (their middle point is connected to ground). A simplified scheme of the whole TFCs system electric circuit is shown in Fig. 9

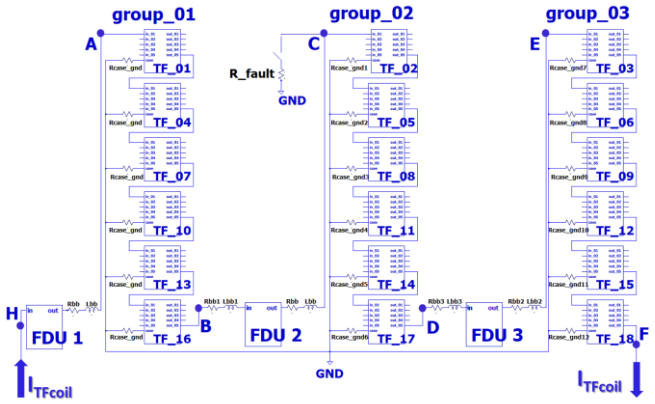

Fig.9. Simplified scheme of TFCs system electric circuit.

V. SIMULATION RESULTS

All simulations have been carried out in *Ansys Simplorer* software environment by setting the transient analysis with a minimum and a maximum time step of 1μs and 100 μs, respectively, and an end time of 200 ms. The rated current value supplies by TFPS is 42.5 kA, but after 1.5 ms from the beginning of the simulation the crowbar is closed to bypass the TFPS. As a consequence, at the time 2 ms an opening signal is sent to the FDU hybrid CB and after 50 ms the discharge begins. Two scenarios have been considered:

- the reference scenario characterized by a normal synchronous operation of three FDUs (without faults);
- the failure scenario characterized by a double fault of one FDU (delayed operation and one of terminals grounded).

For each scenario are reported the voltages across: coils groups, TFCs inside group and DPs inside TFCs, in order to identify the most stressed component in terms of overvoltage both in normal operation and fault conditions.

A. Reference scenario

This scenario describes the regular synchronous switching on of the three FDUs 500 μs after the crowbar is closed. This means that at the time 52 ms the CB of each FDU has completed the opening sequences and each group of coils starts to discharge the stored magnetic energy on the dump resistors. The voltage waveform across each coils group has been computed and is reported in Fig. 10 when $R_{case\text{-}to\text{-}gnd}$ is 100 mΩ.

As expected, the three voltage curves are overlapped because the circuital configuration of each coils group is symmetrical respect to the grounding. The first milliseconds of the voltage waveform across each TFCs group after the FDU complete opening is composed of two parts (Fig 10 and its inset): an initial spike with a high voltage peak (up to 5.33 kV) followed by a damped oscillation around the value of 5 kV up to reach the value of 5.1 kV when the first pair of IGCT triggers to modulate the dump resistance value. Fig. 11 shows the terminal-to-terminal voltage of the six coils belonging to group_01. During the firsts tens of microseconds from the FDUs triggering, the voltage inside the group of six coils is not uniformly distributed: the outermost TF01, TF16 (those closest to the FDUs) and the innermost coils TF07, TF10 have broader oscillations with a maximum value of about 950 V. The other coils instead (TF04, TF13), at the same instant, reach lower maximum values (Fig. 11). The transient evolution of the terminal-to-terminal voltage distribution inside the coil TF01 has been simulated and is showed in Fig. 12.

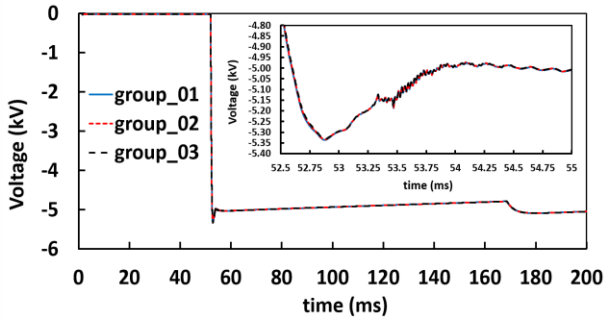

Fig.10. Voltage across coils groups for $R_{case\text{-}to\text{-}gnd}$ =100 mΩ.

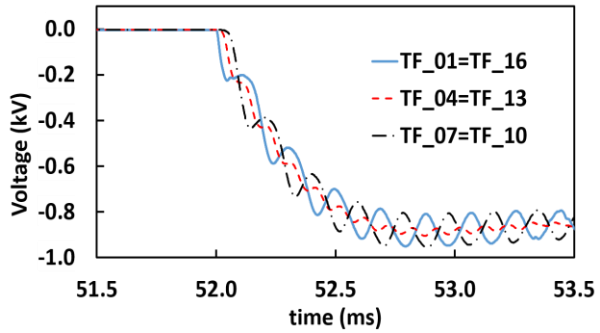

Fig.11. Voltage across TFCs of group_01 for $R_{case\text{-}to\text{-}gnd}$ =100 mΩ.

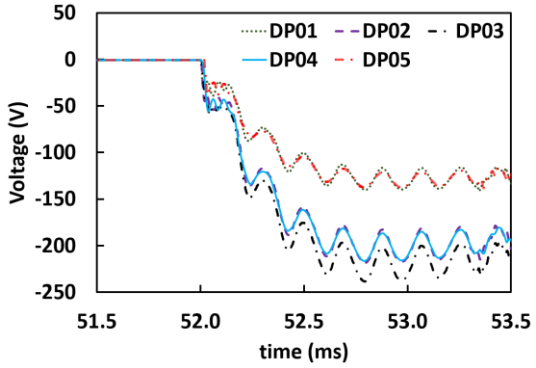

Fig.12. Voltage across DPs inside TF_01 coil for $R_{case\text{-}to\text{-}gnd}$ =100 mΩ.

The voltage distribution across each DP is not uniform due to both, the different number of turns and to their internal position: the DP03 reaches the highest voltage value, about 250 V, during the initial spike. These waveforms are characterized by different and fast oscillations due to the stray capacitances between the turns and the surrounding elements connected to ground. The terminal-to-ground voltage waveform of each coils group have also been computed: knowing this value is important for the correct sizing of the ground insulation of each single component. Due to the symmetrical grounding, the voltage waveform of the plus and minus terminals across each group are only half of the group terminal-to-terminal voltage and reach the same peak value of 2.64 kV (absolute value) at the same instant *t = 52.88 ms*. Since the voltage drop across the busbar is negligible, the terminal-to-ground voltages waveform of each FDU are those seen at the ends of each group.

The terminal-to-ground, $V_{terminal\text{-}to\text{-}gnd}$, voltage distribution for all DPs, the most stressed of the coils, has been computed. With reference to the Fig. 11, these coils are the most external of each group: TF_01 and TF_16 of group_01; TF_02 and TF_17 of group_02; TF_03 and TF_18 of group_03). Fig. 13 shows the obtained voltage waveforms within the TF_01 coil.

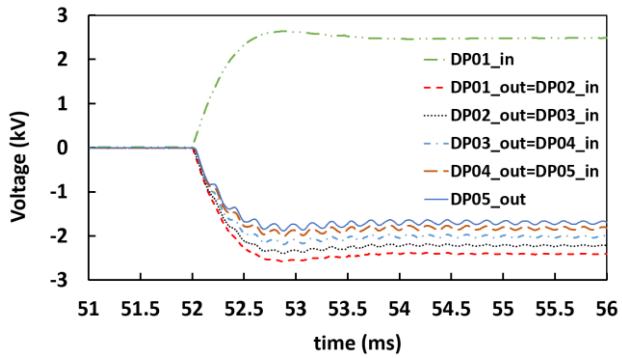

Fig.13. Terminal-to-ground voltage for all DPs within the TF_01 coil.

Different maximum values (1.89 kV÷2.64 kV at 52.88 ms) of the $V_{terminal\text{-}to\text{-}gnd}$ stress the ground insulation inside the WP cross section in the toroidal direction (z-axis in Fig. 3) from DP01 terminal to DP05 terminal.

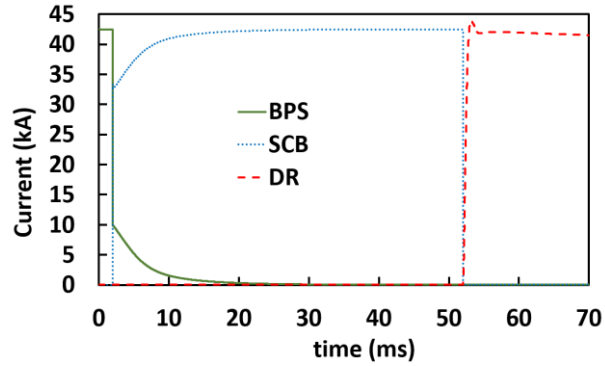

Fig.14. Current commutation between the components inside each FDU.

As can be seen in Fig. 14, inside each FDU the current commutation from SCB to DR (some microseconds) is more critical compared to the commutation from BPS to SCB (some

millisecond) whereas the effect of the stray inductances, L_{stray}, on the voltage waveform is limited by the C_{clamp} presence.

Setting the $R_{case\text{-}to\text{-}gnd}$ of each TFC to 1 mΩ, the transient analysis has been repeated: different values of $R_{case\text{-}to\text{-}gnd}$ up to 100 mΩ do not influence the transient voltage waveforms.

B. *Failure scenario*

In order to investigate the possible overvoltage across TFCs terminals, which can be dangerous for insulation endurance, a double fault condition has been analysed: FDU_2 is switched on with a 5 ms delay with respect to the other FDUs and 10 μs later a ground fault has been simulated. Due to FDUs asynchronous triggering, the highest transient voltage stress in the TFCs happens and a failure of the insulation toward ground is most probable. Therefore, the fault to ground, placed close to FDU_2, has been simulated by means of a resistance, $R_{fault\text{-}to\text{-}gnd}$, of 1 Ω inserted between the C-terminal and ground (Fig. 9). Different voltage waveform oscillations have been observed across each coils group as shown in Fig. 15.

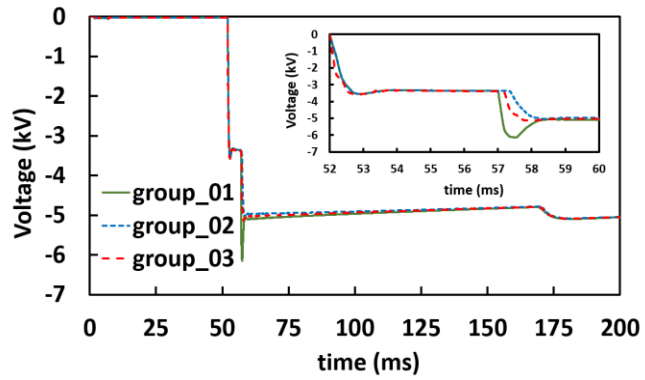

Fig. 15. Voltage across coils groups for $R_{fault\text{-}to\text{-}gnd}$ =1 Ω.

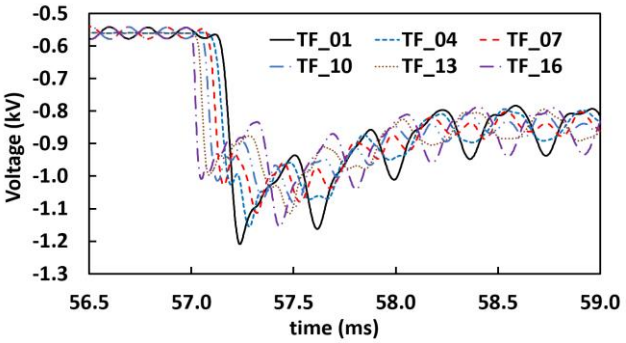

Fig. 16. Voltage across TFCs of group_01 for $R_{fault\text{-}to\text{-}gnd}$ =1 Ω.

Each curve is characterized by two peak values: 3.57 kV (the same for each curve) at the time 52.7 ms when the CBs of FDU_1 and FDU_3 switch the current on their respective DRs; 6.15 kV for group_01 curve at the time 57.5 ms and 5.1 kV for the others curves some milliseconds later. The maximum over-voltage of 6.15 kV occurred across coils group_01 when FDU_2 is switched on and $R_{fault\text{-}to\text{-}gnd}$ = 1 Ω is inserted: then, this curve decreases up to 5.08 kV when the first pair of IGCTs is activated to modulate the DR value. Different voltage waveform oscillations have been also observed across each coil belong to group_01 while the FDUs are switching on (Fig. 16). As can be seen, each voltage waveform has a peak value followed by a series of damped oscillations. The most stressed coil in terms of highest voltage is the TF01: its peak value is 1.21 kV. Similarly, the voltage distribution is not uniform across each DP inside the coil TF01. As discussed earlier, each DP03 is experiencing the higher voltage than the other DPs: for example, DP03 of the TF01 has a voltage of about 300 V (Fig. 17).

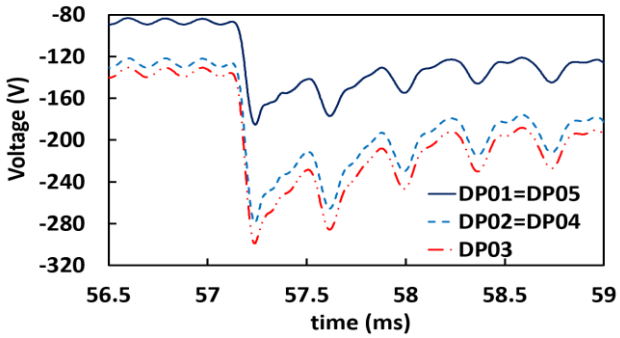

Fig. 17. Voltage across DPs inside TF_01 coil for $R_{fault\text{-}to\text{-}gnd}$ =1 Ω.

The fault ground resistance of 1 Ω introduced in the circuit has an impact even on terminal-to-ground voltage of each coils group. With reference to the terminals A, B, C, D, E and F in Fig. 9, the terminal-to-ground voltages have been computed and are shown in Fig. 18.

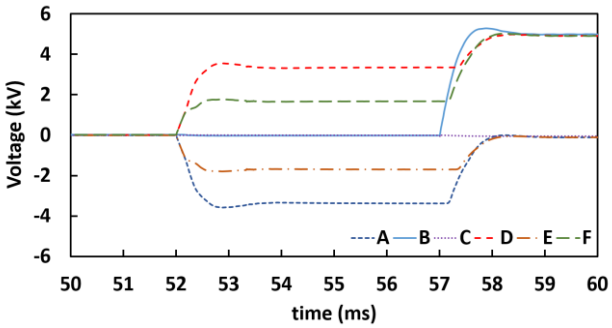

Fig.18. Terminal-to-ground voltage of each coils group for $R_{fault\text{-}to\text{-}gnd}$ =1Ω.

The different behaviour of the terminal-to-ground voltages in the two time ranges can be highlighted:

- from 52 ms to 57 ms: FDU_2 is switched off
- from 57 ms to 62 ms: FDU is switched on and a ground fault occurred.

As can be seen, the C-terminal voltage is associated to the coils group_02 terminal connected to ground (its value is few ten volt) while the voltage of its terminal (D) increase from 3.3 kV up to 5 kV when FDU_2 is switched from off to on. E-terminal and F-terminal curves, associated to the group_03, have equal and opposite voltage values (about 2 kV) until t = 57 ms when FDU_2 is still switched off: then E-terminal decrease to a few tens of volt and the F-terminal voltage increase up to 5 kV. A-terminal and B-terminal associated to the coils group_01, are also unbalanced: A-terminal curve has equal and opposite voltage values to the D-terminal curve when FDU_2 is switched off, but increases up to few tens of volt when FDU_2 is

switched on; the B-terminal curve has the same voltage values as the C-terminal curve until t=57 s, then it reaches a peak value of 5.27 kV at 57.87 ms and afterwards decreases up to 5 kV. As a consequence, the maximum voltages computed for the WP ground insulation of the TF_16 (Fig. 19) are higher than the obtained voltage values for TF_01 in the reference scenario: TF_01 and TF_16 are the outermost coils of the group_01.

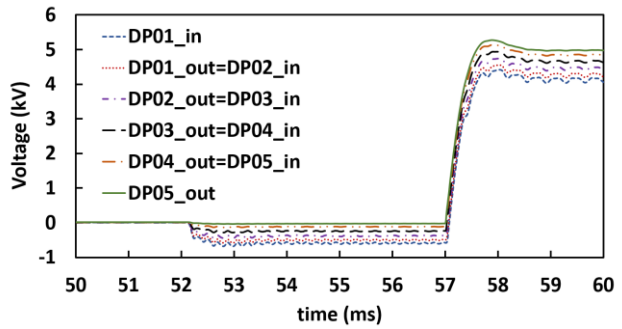

Fig.19. Terminal-to-ground voltage for all DPs within TF_16 coil in failure scenario

The designed allowable voltage stress, $E_{allowable}$, for WP insulation is 10 kV/mm and the chosen safety margin factor, $S = V_{allowable}/V_{service}$ is 3. These choices take into account various effects regarding the insulation system (thermal cycling, mechanical stress, aging, defects and quality of the manufacturing process, and so on) which would tend to decrease the $E_{allowable}$ during service. Therefore, the design values of the WP insulation thickness (see section III.A) should withstand the computed voltages even during the failure scenario (double fault). The S-factor for TF insulating system is associated to the low exposure time to the high voltage, which only occurs during fast discharge operations for quench protection. The transient analysis has been repeated for other two values of $R_{fault\text{-}to\text{-}gnd}$: 10 mΩ and 100 Ω, being the latter value comparable to the earthing resistance connected to the middle point of each dump resistor. The voltage across coils group_01 remains unchanged for the $R_{fault\text{-}to\text{-}gnd}$ value included in the 10 mΩ ÷ 1 Ω range (Fig. 20), whereas it changes for $R_{fault\text{-}to\text{-}gnd} = 100\ \Omega$: its value become 5.40 kV as shown in detail (see Fig.9). Therefore, the fault resistance value starts having a strong impact on the maximum transient voltage when its value is included in 10 mΩ ÷ 1 Ω range.

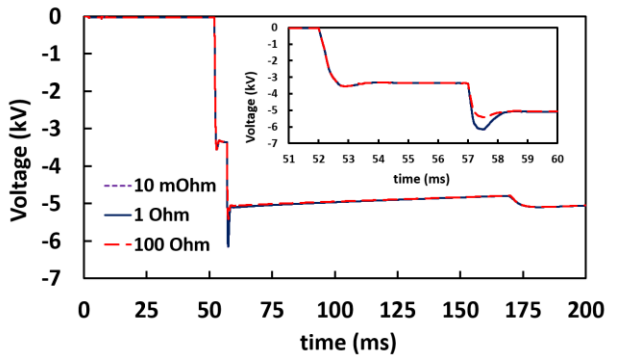

Fig.20. Voltage across coils group_01 for different $R_{fault\text{-}to\text{-}gnd}$ values.

VI. Conclusion

For correct sizing and coordination between the protection system and the magnets insulation, the estimation of the voltage waveforms during transients is very important. A model of the TFCs circuit has been developed to investigate this aspect in case of a fast discharge. In particular, the voltage waveforms and their maximum values have been computed for two scenarios: the simplifications, adopted and included in the model, have produced an overestimation (the amount of which will be the subject of future investigations) of the resulting peak values. It has been found that, in case of synchronous operation of the FDUs (reference scenario), when each TF case is connected to ground by means of a resistance $R_{case\text{-}to\text{-}ground}$, ($1\ m\Omega \leq R_{case\text{-}to\text{-}ground} \leq 100\ m\Omega$), the maximum voltage value across each coils group is 5.33 kV whereas the maximum terminal-to-ground voltage value is 2.64 kV, within the selected values of the stray inductances and clamp capacitor inside of each FDU [18, 19]. Inside each coils group, the maximum terminal-to-terminal voltage value for the outermost coils reaches 950 V with a maximum voltage of about 250 V across DP03. The worst case in terms of terminal-to-terminal and terminal-to-ground insulation has been identified for a double fault (failure scenario) [3] consisting of a triggering delay of FDU_2 with an additional ground fault ($10\ m\Omega \leq R_{fault\text{-}to\text{-}gnd} \leq 1\ \Omega$) at one coils group_02 terminal. In this conditions, the maximum voltage value across each coil can reach the maximum value of 6.15 kV (group_01) whereas inside of the group_01, the maximum terminal-to-terminal voltage value for the TF_01 coil can reach 1.21 kV with a maximum voltage of about 300 V across DP03. The WP insulation of the outermost coils of the group_01 is the most voltage-stressed: the maximum terminal-to-ground voltage for all DPs belonging to TF_16 coil has been computed resulting in 5.26 kV, that is about two times higher than the voltage stresses in the WP insulation of the DPs belonging to the TF_01 coil during the reference scenario. Therefore, with an allowable voltage stress of 10 kV/mm and a safety margin factor of 3, the WP insulation should withstand the computed voltages during the analysed scenarios. The results of the sensitivity analysis have pointed out that both the fault-to ground resistance and the resistance of TF case to ground play an important role on defining the magnitude of over-voltages and on management of a fault to ground. Further, this study allows to address mitigation strategies, in order to reduce electric stress at the insulation level and an increased awareness of protection strategies in different fault conditions. As well known, the simulation currently remains only a preliminary tool. The model described here has been developed and suited for the DTT TFCs design characteristics, based on the lessons learnt in the recent past. DTT cables Model Coils are not available for tests, nevertheless the simulation strategies, implemented here, are based on referred verified assumption [4]-[7], which became milestones for the fusion coils community. Experimental tests on the finished DTT TFCs are, on the other hand, planned in the Cold Test Facility at ENEA Frascati, and it will be then possible to asses, quantify and adjust the specific model parameters.

ACKNOWLEDGMENT

This paper is the result of a strong synergy between the superconductivity group and the power supply group of ENEA in collaboration with Dipartimento di Ingegneria - Università degli Studi di Palermo contributing to the design of TF superconducting magnets and TF power supply system of DTT. International experimental infrastructure on nuclear fusion has been co-funded by European Investment Bank (EIB), Eurofusion, Research and University Ministry, Economic Development Ministry and Lazio Region in 2019. In this framework ENEA has funded a Ph. D. fellowship in electrical engineering at UNIPA to support the R&D activities connected to the design of these components. https://www.dtt-project.it/index.php#.

REFERENCES

[1] R. Martone, R. Albanese, F. Crisanti, A. Pizzuto, P. Martin, "DTT Divertor Tokamak Test facility Interim Design Report," ENEA Frascati Research Center, Italy. Available: https://www.dtt-dms.enea.it/share/s/avvglhVQT2aSkSgV9vuEtw. Apr. 2019.

[2] G.M. Polli et al., "DTT's Role, Characteristics & Design Status," *20th IEEE Mediterranean Electrotechnical Conference, MELECON 2020*, Jul. 2020.

[3] P. Zito, G. Tomassetti, G. Messina, et al., "Conceptual Design and Modeling of the Toroidal Field Coils Circuit of DTT," *20th IEEE Mediterranean Electrotechnical Conference, MELECON 2020*, Jul. 2020.

[4] W.H. Fietz, et al., "Internal Transient Over-Voltages in Large Fusion Coils," *IEEE Transactions on Applied Superconductivity*, vol. 22, Jun. 2012, Art. no. 4704405.

[5] S. Fink, et al., "High Voltage Tests of the ITER Toroidal Field Model Coil Insulation System", *IEEE Transactions on Applied Superconductivity*, vol. 12, Mar. 2002, Art. no. 7346980.

[6] S. Fink, et al., "Transient Electrical Behavior of the ITER TFCs during fast discharge and two fault cases", *Fusion Engineering and Design*, Vol. 75 – 79, Aug 2005, pp. 135 – 138.

[7] C. Meinecke, A M. Miri, A. Ulbricht and S. Fink "Investigation of the transient electrical behavior of the ITER Central Solenoid Model Coil (CSMC) during safety discharge", *IEEE Transactions on Applied Superconductivity*, vol. 12, Aug 2002, Art. no. 7347184.

[8] A. Di Zenobio, et al., "DTT device: Conceptual design of superconducting magnet system", *Fusion Engineering and Design*, Vol. 146, Apr 2017, pp. 299 – 312.

[9] A. Ulbricht et al., "The ITER Toroidal Field Model Coil project", *Fusion Engineering and Design, Vol.* 73, Oct 2005, pp. 189 - 327.

[10] R. Bonifetto et al., "Thermal-Hydraulic Analysis of the DTT Toroidal Field Magnets in DC Operation", *IEEE Transactions on Applied Superconductivity*, Vol. 30, Jun 2020, Art. no. 19419972.

[11] Hartmut Ehmler, Matthias Köppen, "ac modeling and impedance spectrum tests of the superconducting magnetic field coils for the Wendelstein 7-X fusion experiment", *Review of Scientific Instruments*, Vol. 78, Oct 2007, Art. no. 104705.

[12] A. Coletti, et al., "JT-60SA power supply system", *Fusion Engineering and Design*, Vol. 86, Oct. 2011, pp. 1373 – 1376.

[13] A.M. Miri, et al., "Transient Behavior of Superconducting Magnet Systems of Fusion Reactor ITER during Safety Discharge", *Hindawi Publishing Corporation Modelling and Simulation in Engineering*, Vol. 2008, Dec 2008, Art. ID 359210.

[14] L. Novello, et al., "Analysis of Maximum Voltage Transient of JT-60SA Toroidal Field Coils in Case of Fast Discharge", *IEEE Transactions on Applied Superconductivity*, Vol. 26, Mar. 2016, Art. no 4700507.

[15] A. Bruno, et al., "Broadband Electromagnetic Modeling of the Superconducting Toroidal Field Magnets of JT-60SA: Transient Simulation and Fault Detectability", *IEEE Transactions on Applied Superconductivity*, Vol. 27, Aug. 2017, Art. no. 4201608.

[16] L. Novello, E. Gaio, R. Piovan, M. Takechi, S. Ide, M. Matsukawa, "Overcurrent analyses in JT-60SA poloidal circuits due to plasma disruption and quench protection intervention," *Fusion Engineering and Design*, Vol. 86, 2011, pp. 33-40.

[17] A. Maistrello, E. Gaio, L. Novello, M. Matsukawa, K. Yamauchi, "Analyses of the impact of connections' layout on the coil transient voltage at the Quench Protection Circuit intervention in JT-60SA," *Fusion Engineering and Design*, Vol. 98-99, Jul. 2015, pp. 1109-1112.

[18] A. Maistrello, M. Dan, V. Corato, K. Sedlak, E. Gaio, "Preliminary studies on DEMO toroidal field circuit topology and overvoltage estimation," *Fusion Engineering and Design*, Vol. 146, Sep. 2019, pp. 539-542.

[19] C.R. Lopes, P. Zito, C. Fiamozzi Zignani, G. Messina, L. Morici, G. Tomassetti, A. Lampasi, G. Ala, G. Zizzo, "Design Optimization for the quench protection of DTT's Superconducting toroidal field magnets", *Fusion Engineering and Design*, Vol. 172, Nov. 2021.

[20] C. R. Lopes, P. Zito, G. Ala, G. Zizzo, A. Lampasi, "Transient DC Arc voltage model in Hybrid switch of the DTT fast discharge Unit", currently being published for EEEIC 2021. In press

[21] R. Ammerman, T. Gammon, P. Sen. J. Nelson, "DC-arc models and incident-energy calculations", *IEEE Transaction on industry applications*, Vol. 46, Sep/Oct 2010, pp. 1810-1819.

[22] E. Gaio, et al., "The new technological solution for the JT-60SA quench protection circuit", *IOP Publishing Nuclear Fusion*, Vol. 58, Jun. 2018, no. 075001.

[23] Inho Song, et al., "The fast discharge system of ITER superconducting magnets", *IEEE 2011 International Conference on Electrical Machines and Systems*, Nov. 2011, Art. no. 12389465.